Journal of Imaging Science and Technology® 52(2): 020502–020502-10, 2008.

Deposition of Molten Ink Droplets on a Solid Surface

Ri Li, Nasser Ashgriz and Sanjeev Chandra
Department of Mechanical and Industrial Engineering, University of Toronto, 5 King's College Road, Toronto, Ontario, Canada, M5S 3G8
E-mail: ashgriz@mie.utoronto.ca

John R. Andrews
Xerox Corporation, Wilson Center for Research & Technology, 800 Phillips Rd. M/S 114-44D, Webster, New York 14580

Stephan Drappel
Xerox Research Centre of Canada, 2660 Speakman Drive, Mississauga, Ontario, Canada, L5K 2L1

Abstract. *An experimental study on the deposition of micro-size droplets (~39 μm in diameter) of molten wax ink on an aluminum surface is presented. Effects of initial temperature of droplets, substrate temperature and distance from printhead to substrate on the deposited droplet shape and textures were investigated. Depending on impact conditions, droplets may have either smooth or irregular edges, and the final shape may be either regular or two tiered. Analysis was conducted to compare the time scales for solidification, viscous damping and oscillation. A simple heat transfer model was developed, and temperature dependences of viscosity and surface tension were taken into account. The Ohnesorge number of droplets was investigated as a function of time to compare the transient effects of viscous damping and oscillation of the droplets after impact. The number of oscillations completed before the Ohnesorge number reaches unity agrees with the number of tiers formed. The height of the first tier was related to the value of the Ohnesorge number during the first oscillation. The thermal capillary effect was evaluated by defining and examining two Marangoni numbers for the spreading and post-spreading phases of the droplet impact. Splashing of droplets occurred and produced fingers around the droplet peripheries, which was mainly determined by local solidification and spreading dynamics in the vicinity of contact line.*
[DOI: 10.2352/J.ImagingSci.Technol.(2008)52:2(020502)]

INTRODUCTION

Deposition of molten droplets on cold solid surfaces is the key technology for a few industrial applications, which include solid ink jet (SIJ) printing, microfabrication, electronic packaging, rapid prototyping and coating. SIJ printers are widely used to print high quality color images.[1] The solid ink, typically a wax in which colored dyes are dissolved, is ejected in the form of small droplets (20–40 μm diameter) from a heated piezoelectric printhead onto a rotating metal drum. The droplets land on the drum in a pattern that makes up the image and solidify to form hemispherical bumps. The drum is then rolled over a sheet of paper, to which the ink droplets cling, transferring the entire image onto the paper.

The quality of images formed depends on the shape and texture of the wax ink droplets deposited and solidified on the drum.[2] If the deposited droplets are irregular in shape, or excessively flattened, they will not transfer well to the paper. To achieve good print quality requires understanding the mechanism of print conditions affecting the shape of droplets deposited on drum surface. Although there are numerous studies on the impact and solidification of molten drops on cold solid surfaces,[3–5] there are very limited ones in the parametric range of SIJ printers.

This paper presents results of a study on the impact and solidification of small molten wax droplets on a solid surface in the typical parametric range of SIJ printers. Droplet shape and its surface texture after impact and solidification were studied for a range of initial droplet temperature, substrate temperature and distance from printhead to substrate. Scanning electron microscope (SEM) images were taken of the deposited droplets.

EXPERIMENTAL METHOD

Figure 1 shows a droplet, initially at the temperature of the printhead (T_j), being ejected towards the substrate at temperature T_s. The main purpose of the present study is to provide information on droplet impact in the parametric range relevant to SIJ printers. Therefore, droplets were generated using a commercial printhead, Phaser 860 (Xerox Corporation, Rochester, NY). This is a piezo-electrically driven droplet generator that can operate based on drop-on-demand technologies.[6] The printhead generates droplets horizontally towards a substrate. A polished aluminum plate (50 mm × 5 mm × 5 mm in size) mounted on a movable platform was used as the substrate. The average roughness of this plate was 0.05 μm. After each droplet was deposited, the stage was moved by 150 μm so as to deposit the next droplet on a clean portion of the surface. Both printhead and substrate were heated with cartridge heaters inserted into them, and their temperatures were regulated with an accu-

Received Jun. 25, 2007; accepted for publication Dec. 4, 2007; published online Apr. 2, 2008.
1062-3701/2008/52(2)/020502/10/$20.00.

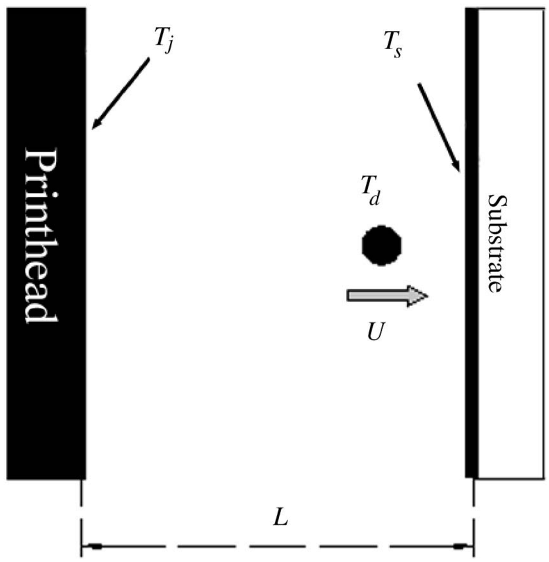

Figure 1. Schematic of the experimental setup showing that a droplet is generated by a printhead, travels a distance L and impacts on a solid surface.

racy of $\pm 0.5°C$ using temperature controllers. Substrate temperature, T_s, was varied from 60 to 80°C in increments of 5°C. Printhead temperature was maintained at either 140 or 145°C, which is referred to as jetting temperature, T_j.

The droplet material, ColorStix 8200 manufactured by Xerox Corporation (Rochester, NY), is a typical commercially used wax-based ink with a complex mixture of components, including crystalline and amorphous waxes with dyes added for color. Various components of this ink have melting points ranging from 60 to 115°C. Variation of the dynamic viscosity (μ) of this ink with temperature is plotted in Fig. 2. The viscosity of the wax ink shows a sharp increase when temperature drops below 95°C, which can be considered as the effective melting point of the material (T_m). For temperature above T_m, the following correlation can be obtained from Fig. 2:

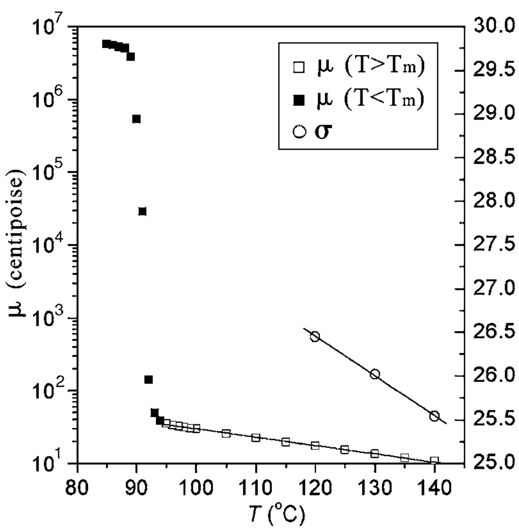

Figure 2. Dynamic viscosity and surface tension of ColorStix 8200 varying with temperature. The two solid lines are linear fittings, and correspond to the correlations shown by Eqs. (1) and (2).

$$\log \mu = 2.6276 - 0.0115\ T, \qquad (1)$$

where μ is in centipoise.

Surface tension (σ) of this ink changes with temperature above the melting temperature: the surface tension of ColorStix 8200 was measured to be 25.54 mN/m at 140°C and 26.45 mN/m at 120°C (Fig. 2). Carrying out linear fitting gives

$$\sigma = 31.918 - 0.0455\ T, \qquad (2)$$

where σ is in mN/m. Some other physical properties of this ink are: thermal conductivity k_d=0.18 W/m K; density ρ=820 kg/m^3; specific heat C_p=2.25 kJ/(kg K); latent heat of fusion L_f=183 kJ/kg. Thermal conductivity of the aluminum substrate is k_s=177 W/m K. All these properties are assumed to be constant, being independent of temperature.

Knowing the effective melting temperature of the ink, the substrate temperature T_s can be represented in dimensionless form by the Stefan number:

$$\mathrm{Ste} = \frac{C_p(T_m - T_s)}{L_f}. \qquad (3)$$

For substrate temperature T_s ranging from 60 to 80°C, Ste varies from 0.43 to 0.18.

The distance of droplet travel, L, was kept at either 0.5 or 1.0 mm, resulting in droplet velocities (U) of 2.81 ± 0.07 and 2.56 ± 0.04 m/s, respectively. Droplet diameter (D_0) was measured to be 39 ± 0.4 μm. After a droplet landed on a cold surface ($T_s < T_m$), it was allowed to stay at the substrate temperature for approximately 5 min, and then allowed to cool to room temperature. Photographs showed that there was no observable change in the shape of the droplet during this cooling period. Solidified droplets were examined using both optical and scanning electron microscopy (SEM). Droplets were sputter coated with gold before being placed in the SEM, and their temperature was kept well below 60°C during the coating process to avoid any phase change.

Air temperature in the gap between the substrate and printhead was measured using a 0.3-mm-dia thermocouple probe (HYP-1, Omega Engineering, Stamford, CT) mounted on a micrometer stage. Cooling of droplets due to forced convection was calculated by neglecting temperature gradients within droplets (the Biot number was less than 0.1) and using measured values of droplet velocities and air temperatures. The temperature of droplets at the instant of impact upon the substrate is T_d. Results showed that droplets cooled from an initial temperature of T_j=140°C to T_d=136°C at L=0.5 mm and to T_d=132°C at L=1 mm. These values were assumed to be initial droplet temperatures at the time of impact. Increasing jetting temperature T_j from 140 to 145°C did not cause measurable changes of droplet size and velocity. For T_j=145°C, T_d was calculated to be 141°C at L=0.5 mm and 137°C at L=1 mm.

EXPERIMENTAL RESULTS

The shape and size of solidified droplets formed on the substrate were sensitive to substrate temperature. As substrate

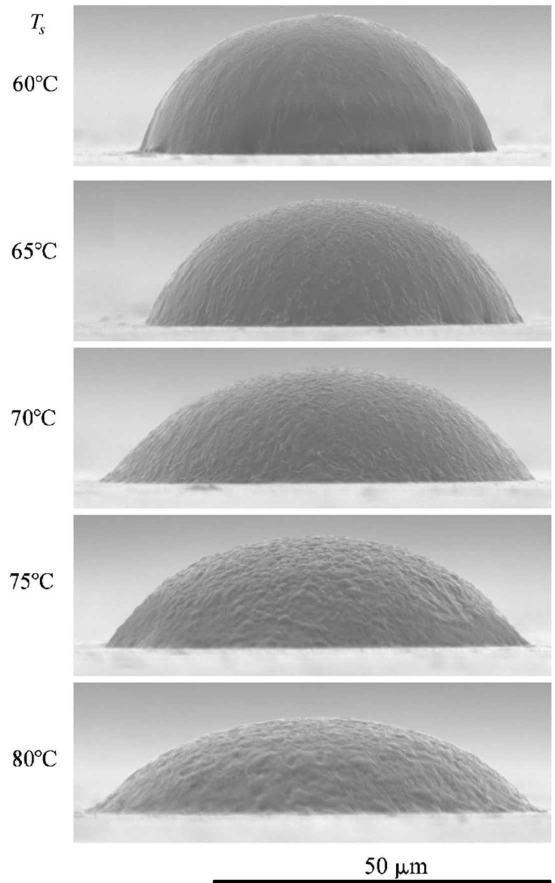

Figure 3. Side view SEM images of wax ink droplets impacted on the aluminum plate (L=1 mm, T_j=140°C).

temperature increased, droplets spread out to a greater extent, so that the base diameter increased and the height of the droplets decreased. Figure 3 shows SEM images of wax droplets impacted on the bare aluminum surface at temperatures ranging from 60 to 80°C (L=1 mm, T_j=140°C), in which the flattening of droplets at elevated substrate temperature is clearly visible. Figure 4 shows measurements of the base diameter (D_s) and height (h) of the droplets normalized by the initial droplet diameter (D_o), and solidification contact angle at the edges of the droplets at varying substrate temperatures and Stefan numbers (Ste, where increasing Ste corresponds to decreasing T_s). Each data point represents an average of five measurements, while error bars mark the maximum and minimum diameters measured. Lines of best fit are shown. As T_s increased (decreasing Ste), the base diameter increased from 1.37 to 1.74 [Fig. 4(a)], the height decreased from 0.53 to 0.38 [Fig. 4(b)] and the solidification contact angle decreased from 77 to 29° [Fig. 4(c)].

The final shape of a droplet landing on a surface depends on physical properties such as viscosity, surface tension and liquid–solid contact angle, all of which depend on temperature. Equilibrium contact angle was measured by placing pieces of wax (with mass ~0.2 mg) on a heated substrate, letting it melt and photographing the equilibrium shape of the molten droplet formed on the substrate. The

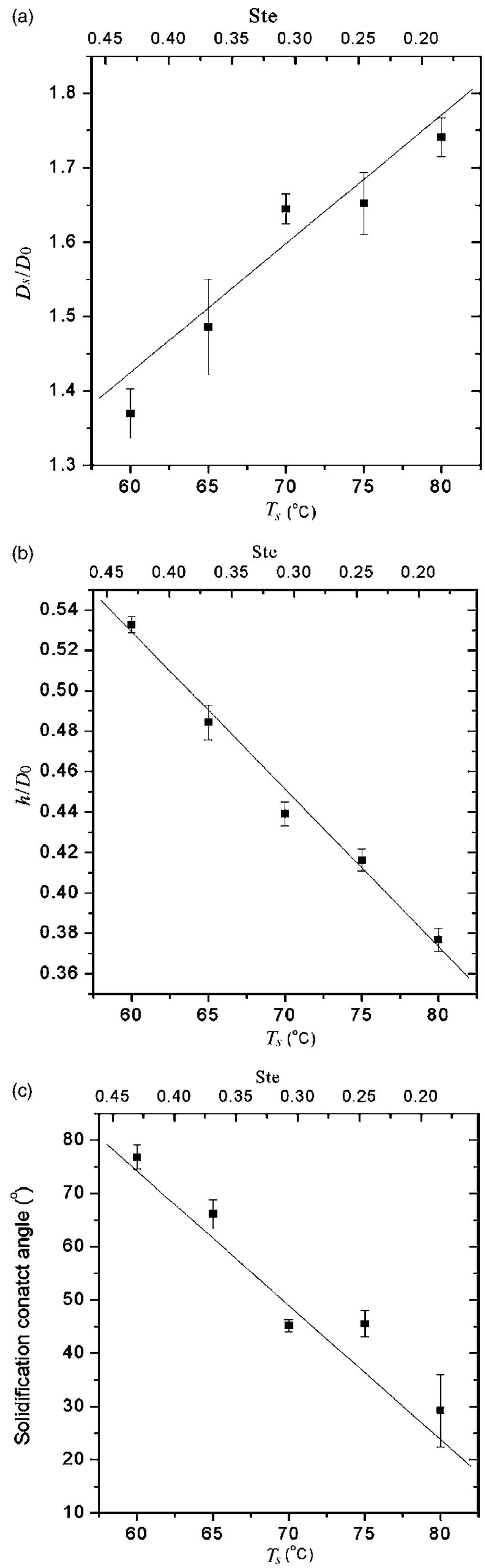

Figure 4. Measurements of final shape of droplets formed on the aluminum plate (L=1 mm and T_j=140°C) varying with substrate temperature (bottom axis) and Stefan number (top axis) Ste=$C_p(T_m-T_s)/L_f$. Simple linear fitting was conducted to better show the tendencies. (*a*) Base diameter. (*b*) Height. (*c*) Solidification contact angle.

equilibrium contact angle of the wax on aluminum surface was approximately 1°, showing good wettability.

The contact angles made by solidified droplets, as shown in Fig. 4(c), were larger than those measured for liquid droplets sitting on heated surfaces, suggesting that they had not reached their equilibrium shape before their movement was arrested. Droplet spreading is driven by inertial forces, and the time required for spreading of a liquid droplet (t_{spr}) can be estimated by[7]

$$t_{\mathrm{spr}} = \frac{D_0}{U} \tag{4}$$

For the experimental conditions in this study $t_{\mathrm{spr}} \sim 15\ \mu\mathrm{s}$.

Gao and Sonin[8] proposed a simple model to estimate the solidification time (t_{solid}) of a molten droplet impacting on a cold solid surface:

$$t_{\mathrm{sol}} \approx \frac{2D_0^2}{3\alpha_d}\frac{k_d}{k_s}[\ln(\lambda + 1) + \mathrm{Ste}^{-1}] + \frac{D_0^2}{3\alpha_d}\mathrm{Ste}^{-1}, \tag{5}$$

where α_d is the thermal diffusivity of droplet and λ the dimensionless superheat parameter:

$$\lambda = \frac{T_d - T_m}{T_m - T_s}. \tag{6}$$

In our experiments, the ratio of thermal conductivities is $(k_d/k_s) \sim 10^{-3}$ and hence the first term in Eq. (5) is negligible. It can, therefore, be simplified to give:

$$t_{\mathrm{sol}} \approx \frac{D_0^2}{3\alpha_d}\mathrm{Ste}^{-1} \tag{7}$$

Combining Eqs. (4) and (7) provides the ratio of the spreading and solidification times:

$$\frac{t_{\mathrm{spr}}}{t_{\mathrm{sol}}} \approx 3\frac{\mathrm{Ste} \cdot \mathrm{Oh} \cdot \mathrm{We}^{0.5}}{\mathrm{Pr}}, \tag{8}$$

where in our tests the Weber number ($\mathrm{We} = \rho U^2 D_0/\sigma_0$) was approximately 8, Ohnesorge number [$\mathrm{Oh} = \mu_0(\rho D_0 \sigma_0)^{-0.5}$] was 0.36, and Prandtl number ($\mathrm{Pr} = \mu_0 \mathrm{C_p}/k_d$) was around 130. Here μ_0 and σ_0 represent viscosity and surface tension of the droplet at the instant of impact, i.e., $\mu_0 = \mu(T = T_d)$, $\sigma_0 = \sigma(T = T_d)$. Substitution into Eq. (8) gives $t_{\mathrm{spr}}/t_{\mathrm{sol}} < 10^{-2}$, indicating that the spread time is two orders of magnitude lower than the solidification time. From this analysis we can conclude that the droplet would solidify completely long after it had spread to its maximum extent.

However, even when a droplet spreads to its maximum extent, it does not necessarily come to rest, but may recoil. The time for recoil (t_{rec}) can be approximated by half the linear oscillation period of droplet (t_{osc}) given by[9,10]

$$t_{\mathrm{osc}} = \left(\frac{\rho D_0^3}{\sigma_0}\right)^{0.5} \tag{9}$$

and hence,

$$t_{\mathrm{rec}} = \frac{1}{2}\left(\frac{\rho D_0^3}{\sigma_0}\right)^{0.5}. \tag{10}$$

Viscous forces oppose the recoiling motion, and the viscous damping time (t_{damp}) is[7]

$$t_{\mathrm{damp}} = \frac{\rho D_0^2}{\mu_0} \tag{11}$$

Then, the total impaction time (t_{imp}) is

$$t_{\mathrm{imp}} = t_{\mathrm{spr}} + t_{\mathrm{rec}}, \tag{12}$$

which is the time taken for the droplet to spread and recoil. Combining Eqs. (4) and (10)–(12) gives

$$\frac{t_{\mathrm{imp}}}{t_{\mathrm{damp}}} = \frac{\mathrm{We}^{0.5} + 2}{2\ \mathrm{Re}}, \tag{13}$$

where the Reynolds number ($\mathrm{Re} = \rho U D_0/\mu_0$) was approximately 7 in our tests. In the present work the ratio $t_{\mathrm{imp}}/t_{\mathrm{damp}} \sim 0.3$, indicating that the time for viscous damping of droplet oscillations is of the same order of magnitude as that of the time for droplet spreading and recoil. As the substrate temperature increases, the viscous effect decreases, thereby resulting in larger spread [Fig. 4(a)]. Bhola and Chandra[11] observed that the shape of millimeter sized wax droplets falling on a solid plate depends on substrate temperature. They concluded that, based on a simple droplet impact model, the change was not due to solidification but the increase of viscosity due to decreasing temperature. It appears that the same conclusion is valid for the micrometer sized droplets of the wax ink.

The final shape of impacted droplets proved to be sensitive to substrate temperature. Figure 5 shows SEM images, viewed from above, of wax droplets after impacting the aluminum substrate held at temperatures ranging from 60 to 80°C. Two columns of photographs are shown: those on the left [Fig. 5(a)] were for the substrate held at a distance $L = 0.5$ mm from the printhead and those on the right [Fig. 5(b)] for $L = 1$ mm. The droplets deposited at $L = 1$ mm are round and circular with smooth textures, and show the increase in base diameter with substrate temperature described earlier [compare Figs. 3 and 4(a)]. However, droplets deposited after traveling a shorter distance ($L = 0.5$ mm) have relatively rough surface textures with irregular edges, for $T_s < 70$°C. The effect of flight distance, L, diminishes as the substrate temperature increases. The images shown in Fig. 5 demonstrate that both the distance L and substrate temperature had significant effects on the deformation of droplets.

Changing the jetting temperature (T_j) also changed the shape of droplets deposited. Figure 6 shows SEM images of droplets deposited with the jetting temperature maintained at 145°C, slightly higher than the temperature of 140°C used for the droplets previously shown in Fig. 5. Images are shown for droplets impacted on the substrate at temperatures ranging from 60 to 80°C, with L of both 0.5 and

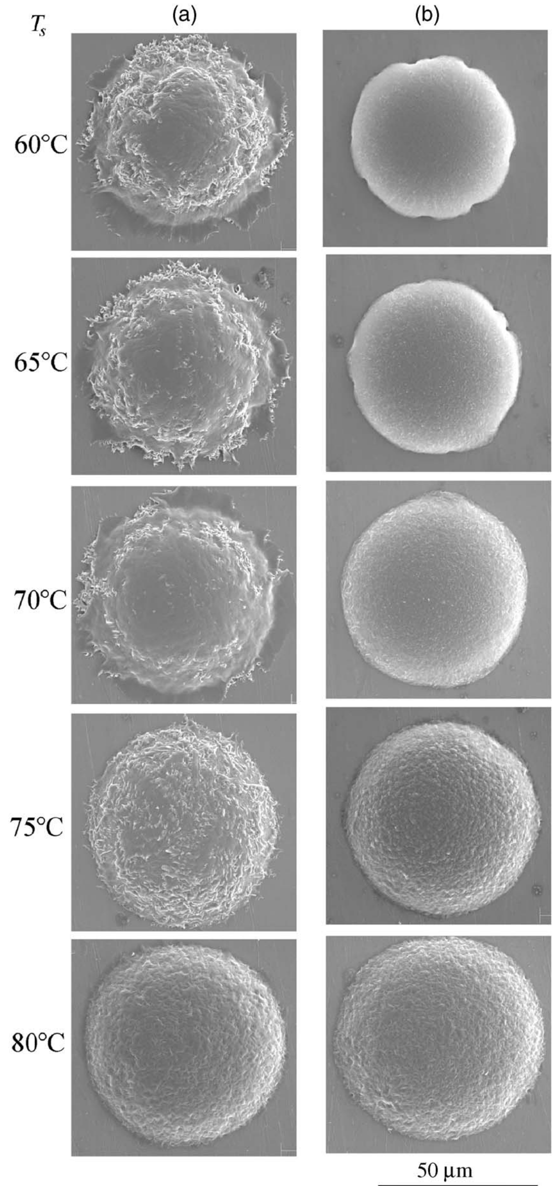

Figure 5. Top view SEM images of wax ink droplets deposited on the aluminum plate (T_i=140°C): (*a*) L=0.5 mm; (*b*) L=1 mm.

1 mm. At $L=0.5$ mm [Fig. 6(a)] the droplets appear to be two-tiered, with a rounder center section surrounded by a wider "skirt." The skirt became smaller as the substrate temperature increased. The two-tiered structure is clearly visible in side views of the same droplets, shown in Fig. 7. When L was increased to 1 mm [Figs. 6(b) and 7(b)] a very narrow skirt was visible at the higher surface temperatures, but disappeared at $T_s=60°$C. Long fingers radiated out from the droplets at higher surface temperatures [Fig. 6(b)].

Figure 8 shows that the base diameter D_s increases with T_s for $L=1$ mm, but an opposite trend is shown for $L=0.5$ mm. This could be caused by the retraction of contact line during the droplet recoil. At $L=0.5$ mm, droplets have both higher impact velocity and temperature than those with $L=1$ mm. They spread to their maximum extent and were pulled back by surface tension before the contact line was arrested. As substrate temperature increased for $L=0.5$ mm, the arrest of contact line was delayed, resulting in decreased base diameters.

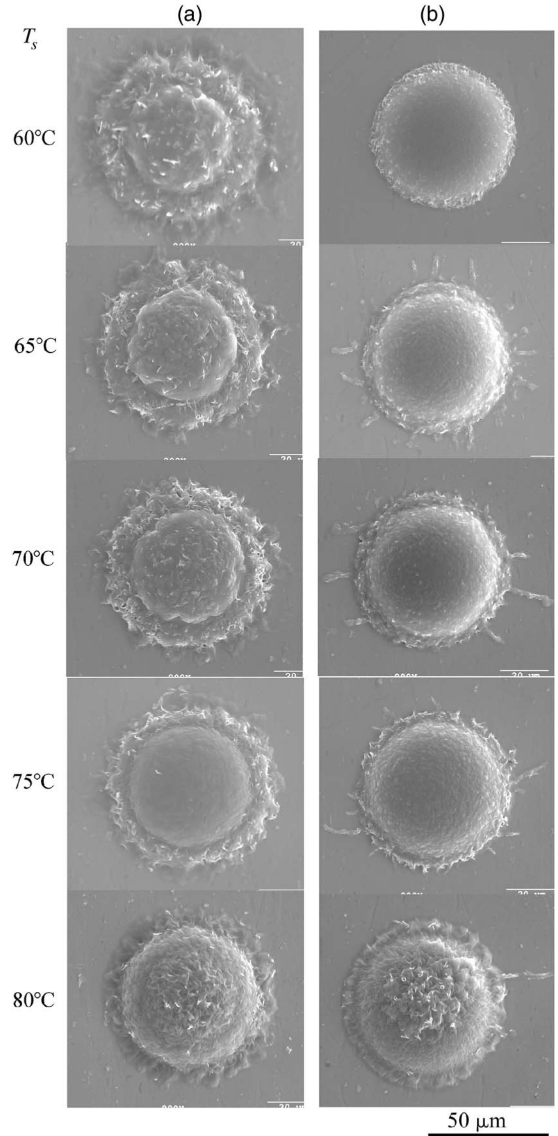

Figure 6. Top view SEM images of wax ink droplets impacted on the aluminum plate (T_i=145°C): (*a*) L=0.5 mm; (*b*) L=1 mm.

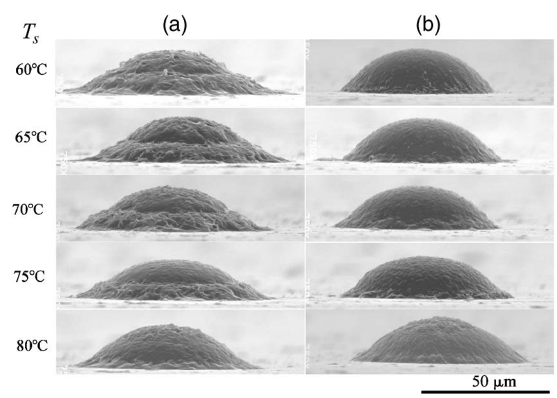

Figure 7. Side view SEM images of wax ink droplets formed on the aluminum plate (T_i=145°C): (*a*) L=0.5 mm; (*b*) L=1 mm.

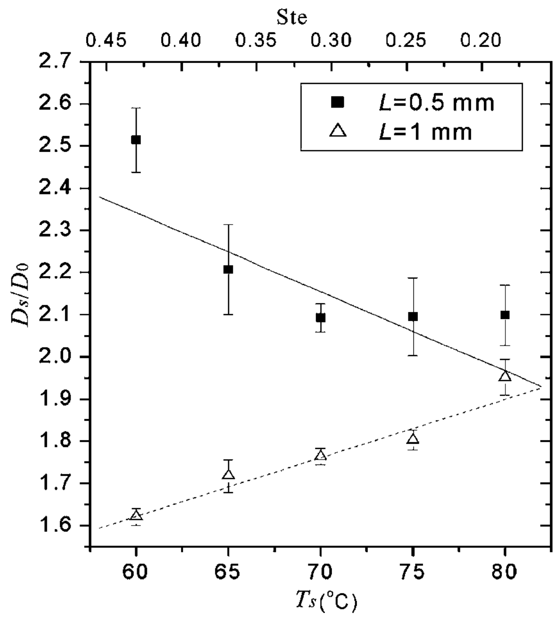

Figure 8. The base diameters of droplets with T_j=145°C.

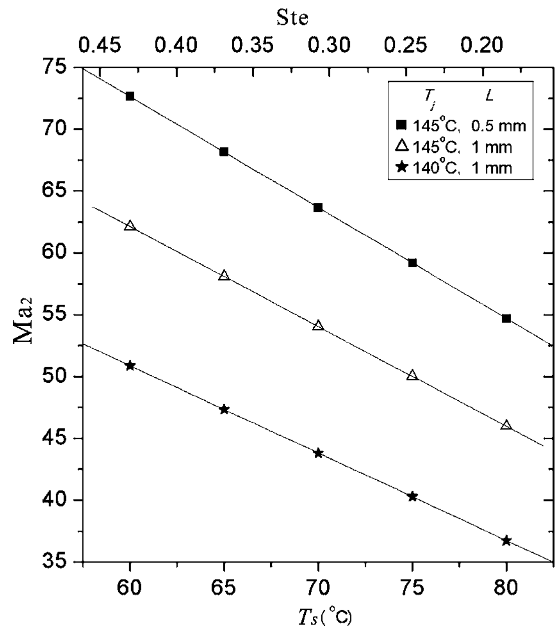

Figure 9. Thermal Marangoni number of droplets in post-spreading phase [Eq. (16)].

Thermocapillary flows may also affect droplet shape after impact and spreading on a cold surface. To evaluate this effect, we consider two thermal Marangoni numbers, one for the spreading phase denoted by Ma_1, and the other one for the post-spreading phase denoted by Ma_2. The thermal Marangoni number compares the velocity of capillary driven flows to the velocity of other transport phenomena in the droplet. The characteristic velocity due to thermocapillary flows is:

$$V_\sigma = \frac{d\sigma}{dT}\frac{(T_s - T_d)}{\mu_0}. \tag{14}$$

During impact the speed of mass transport within the droplet is of the same order of magnitude as the impact velocity and the Marangoni number can be defined as[12]

$$\mathrm{Ma}_1 = \frac{V_\sigma}{U} = \frac{\mathrm{Re}}{\mathrm{We}}\frac{d\sigma}{dT}\frac{(T_s - T_d)}{\sigma_0}. \tag{15}$$

The numerical results of Dietzel et al.[12] showed that contact lines are arrested due to solidification for $\mathrm{Ma}_1 < 19$, and that the arrest of contact line is dominated by surface tension for $\mathrm{Ma}_1 > 19$. Since $0.07 < \mathrm{Ma}_1 < 0.13$ in the present work, it can be concluded that the thermal Marangoni effect had negligible effect on the droplet spreading dynamics.

Previous studies (Ehrhard and Davis,[13] Ehrhard[14]) have shown that cooling the substrate under an initially stationary droplet makes it spread further due to Marangoni flows driven by surface tension variations in it, which are induced by temperature gradients. The strength of such thermocapillary flows, when there is no bulk velocity in the drop, can be estimated from a Marangoni number defined as

$$\mathrm{Ma}_2 = \frac{V_\sigma}{\alpha_d/D_0} = \frac{d\sigma}{dT}\frac{(T_s - T_d)D_0}{\mu_0\alpha_d}, \tag{16}$$

which compares the thermocapillary flow velocity to the speed of thermal diffusion. Values of Ma_2, calculated for the droplets in Figs. 5 and 6, are shown in Fig. 9. Values of Ma_2 lie between 35 and 75, showing that significant thermocapillary flows exist in droplets after they have come to rest on the substrate. The larger the temperature difference between the droplet and substrate, the stronger are surface tension driven flows, which may account for the difference between the measured base diameters in Fig. 8. The final diameter will be a result of droplet impact, recoil and subsequent thermocapillary driven spreading. As the surface temperature increases, temperature gradients within the droplet and consequently the magnitude of thermocapillary forces will decrease.

The formation of a skirt around the ink bumps may be due to oscillation in droplets after impact. Multi-tiered shapes have been reported in a few early works on low Weber number impacts of metal droplets on colder surfaces, including mercury droplets deposited on frozen mercury (Schiaffino and Sonin[7]), pileup of solder droplets (Haferl and Poulikakos[15]) and deposition of single solder droplets (Waldvogel and Poulikakos,[16] Predtechensky et al.[17]). In all these works, the time scales for droplet vibration and solidification were comparable, so droplets froze while still oscillating. The number and size of tiers found on the droplet surface depended on both the time period of oscillations following impact and the rate of solidification (Predtechensky et al.,[18,19] Waldvogel and Poulikakos[16]). To determine whether a similar mechanism controls the formation of skirts around ink droplets, the heights of skirts for droplets produced with a jetting temperature of 145°C were

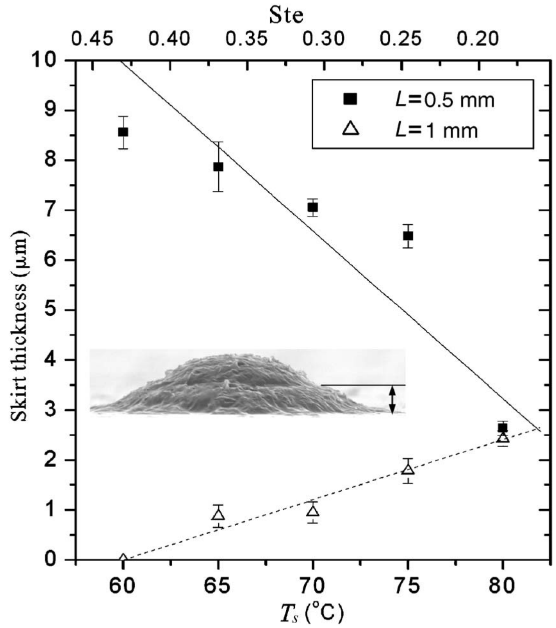

Figure 10. Thickness of skirts formed on the droplets with $T_j = 145°C$.

measured and plotted in Fig. 10 as a function of substrate temperature. For droplets traveling $L=0.5$ mm, the skirt thickness decreased with increasing substrate temperature, whereas for $L=1$ mm this trend was reversed, increasing with T_s.

For molten droplets deposited on cold substrates, three transient physical processes precede the formation of final shapes: viscous damping, oscillation and solidification. Combining Eqs. (7) and (11) gives

$$\frac{t_{\mathrm{damp}}}{t_{\mathrm{sol}}} = \frac{3\mathrm{Ste}}{\mathrm{Pr}}, \tag{17}$$

which is ~0.01 for our cases, showing that viscous damping arrests droplet motion long before they solidify completely. Skirts are formed during droplet impact, spread and recoil. As droplets recoil, their lower part in contact with the substrate cools and its viscosity increases sufficiently to arrest motion. In this portion, surface tension cannot overcome viscosity and fluid flow stops, while the upper portion of the droplet remains fluid enough for surface tension to pull it back into a rounded cap. Since both surface tension and viscosity are extremely sensitive to temperature, it becomes important to know the transient temperature distribution inside a droplet deposited on a surface.

The heat transfer in early analytical models (e.g., Madejski,[3] Pasandideh-Fard et al.[20] and Schiaffino and Sonin[7]) was approximated as one dimensional heat conduction in two semi-infinite bodies. The temperature inside a droplet is one dimensional for low velocity impact (Waldvogel and Poulikakos[16]), but becomes appreciably two dimensional when the heat transfer time scale is comparable to the droplet deformation time scale (Zhao et al.[21]). In the present case the Peclet number $\mathrm{Pe} = D_0 U / \alpha_{\mathrm{d}} \sim 500$, implying that the droplet spreading would be complete long before

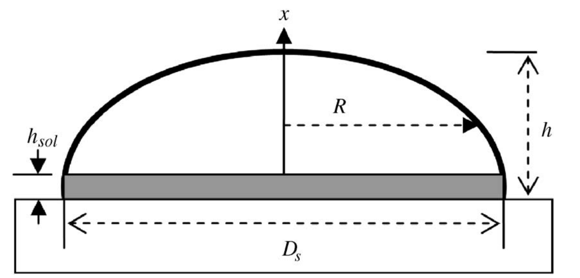

Figure 11. Droplet is assumed to be a spherical cap sitting on substrate. The dark area represents solidified part in the droplet.

significant heat conduction occurred. Additionally, Fig. 9 shows that the values of Ma_2 are less than 80 (Pearson[22]), and heat conduction, therefore, dominates inside the droplet after spreading. Since assuming the droplet and substrate as two semi-infinite bodies underestimates the cooling of the droplet (Amon et al.[23]), we model the droplet with height h (Fig. 11) as a finite slab of thickness h and consider one-dimensional heat conduction inside the slab.

Estimates show that the internal thermal resistance of an ink droplet is three orders of magnitude higher than that of aluminum plate and more than an order of magnitude lower than that of the ambient air. Therefore, we can model the cooling droplet as a slab of finite thickness with one boundary insulated (ink-air interface) and the other at constant temperature (ink-aluminum interface). The one-dimensional heat conduction equation can be solved with these boundary conditions using the method of Bulavin and Kashcheev[24] to get a transient temperature distribution:

$$\frac{T(x,t) - T_s}{T_d - T_s} = \sum_{n=1}^{\infty} \frac{4}{(2n-1)\pi} \times \exp\left(- \frac{(2n-1)^2 \pi^2}{4} \frac{\alpha_d t}{h^2} \right) \sin\left[\frac{(2n-1)\pi}{2} \frac{x}{h} \right], \tag{18}$$

where x is the distance from the ink-substrate interface, as shown in Fig. 11.

Equation (18) is plotted in Fig. 12 as a function of x/h for several dimensionless time points $\alpha_d t / h^2$ (equivalent to Fourier number), showing transient temperature profiles of the droplet after impact. The solidification front (assumed to correspond to $T_m = 95°C$) can be implicitly calculated from Eq. (18) as

$$h_{\mathrm{sol}} = x_{T=T_m}. \tag{19}$$

The solidified layer is extremely thin, remaining much smaller than the skirt thickness during the time the droplet spreads and recoils. Therefore, it cannot account for skirt formation.

The droplet shape is assumed to be a spherical cap, and its dimensions can be determined based on the measured base diameter D_s and the initial diameter D_0, where,

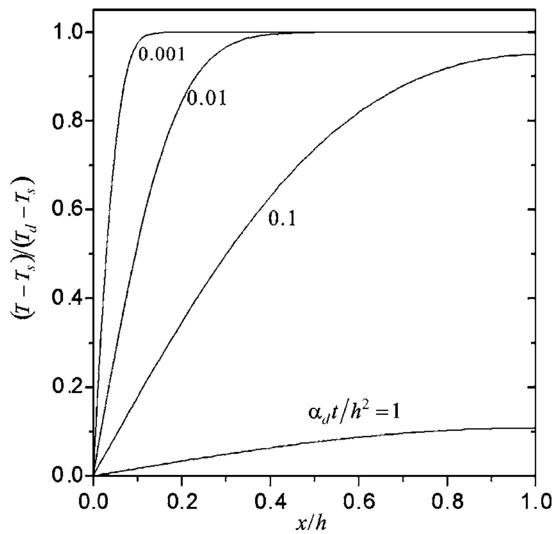

Figure 12. Temperature profiles inside droplets at different dimensionless time points after impact.

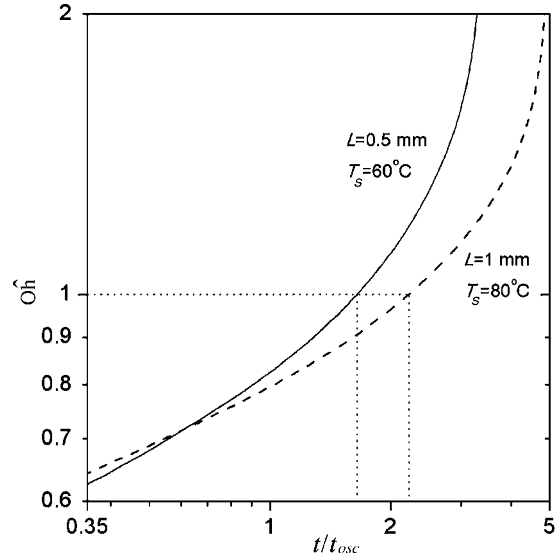

Figure 13. Log-log plotting of Ohnesorge number of droplet as a function of time. As shown by the dotted lines, when $\hat{Oh}=1$, $t/t_{osc}\sim 2$.

$$\frac{3}{4}D_s^2 h + h^3 - D_0^3 = 0 \tag{20}$$

and the radius of the droplet surface is given by:

$$R = \sqrt{\frac{D_s^2}{4} - x\left(\frac{D_s^2}{4h} - h\right) - x^2}. \tag{21}$$

To compare the relative magnitude of viscous and surface tension forces, we evaluate the Ohnesorge number of the remaining liquid in the droplet, above the solidified layer in contact with the substrate (i.e., $h_{\mathrm{sol}}<x<h$).

$$\hat{\mathrm{Oh}} = \frac{\hat{\mu}}{\sqrt{\rho\hat{D}\hat{\sigma}}} \tag{22}$$

Here $\hat{\mu}$ and $\hat{\sigma}$ represent the volume averaged viscosity and area averaged surface tension of the remaining liquid in the droplet at time t, which can be estimated by

$$\hat{\mu} = \int_{h_{\mathrm{sol}}}^{h} R^2\mu dx \Big/ \int_{h_{\mathrm{sol}}}^{h} R^2 dx, \tag{23}$$

$$\hat{\sigma} = \int_{h_{\mathrm{sol}}}^{h} R\sigma dx \Big/ \int_{h_{\mathrm{sol}}}^{h} R dx. \tag{24}$$

The length scale $\hat{D}$ in Eq. (22) is determined from the volume of the remaining liquid

$$\hat{D} = \left(6\int_{h_{\mathrm{sol}}}^{h} R^2 dx\right)^{1/3}. \tag{25}$$

Combining Eqs. (18)–(25) gives $\hat{\mathrm{Oh}}$ as a function of time, which was numerically calculated and plotted in Fig. 13 for two test conditions. In Figure 13, the time t is normalized by t_{osc} given in Eq. (9). Figure 13 shows that the viscous damping effect increases significantly as time t increases. When $\hat{\mathrm{Oh}}$ exceeds unity, the oscillation of the remaining liquid in the droplet is completely damped out and terminated. This explains the smooth texture formed on the top of deposited droplets as shown in Figs. 6 and 7. In Fig. 13, for $\hat{\mathrm{Oh}}=1$, $t/t_{\mathrm{osc}}\sim 2$. This indicates that around two oscillations had occurred before the droplet completely reached its static state. This number of oscillations agrees with the number of tiers observed in Figs. 6 and 7.

Due to viscous dissipation, the oscillation amplitude decreases substantially with time (Bechtel et al.,[10] Predtechensky et al.[19]). Hence, the skirt thickness shown in Fig. 12 is mainly determined by the first oscillation, i.e., $t=t_{\mathrm{imp}}$. The values of Ohnesorge number at $t=t_{\mathrm{imp}}$ were calculated and presented in Fig. 14. The Ohnesorge number decreases with T_s for $L=0.5$ mm and shows a reversed trend for $L=1$ mm. The values of Ohnesorge number for $L=0.5$ mm are larger than those for $L=1$ mm. A large value of Ohnesorge number indicates relatively slow oscillation, which results in higher skirt thickness.

Droplets impacted at $T_j=140°\mathrm{C}$ and $L=1$ mm are smooth without any skirts (Fig. 3). However, the values of Ohnesorge number for this case, which were not presented, are close to those for $T_j=145°\mathrm{C}$ and $L=1$ mm. It should be noted that the Ohnesorge number analysis above did not provide information on the oscillation amplitude, since the impact inertia was not included. Due to the lower impact velocity and initial temperature for $T_j=140°\mathrm{C}$ and $L=1$ mm, droplets may oscillate with small and quickly damped amplitudes, or they may not even oscillate after spreading (Bechtel et al.[10]).

Droplets deposited with $T_j=145°\mathrm{C}$ and $L=1$ mm developed long radial fingers around their peripheries. There were no fingers for $T_s=60°\mathrm{C}$ and very few for $T_s=80°\mathrm{C}$ [Fig. 6(b)]. Bhola and Chandra[11] showed that the number of

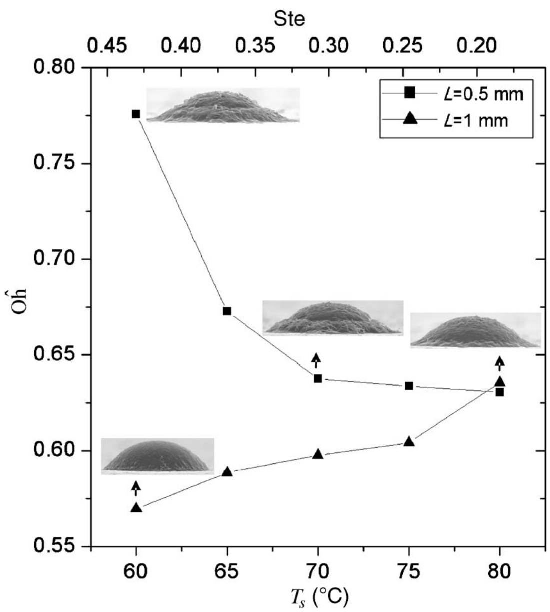

Figure 14. Ohnesorge number at $t=t_{imp}$ for droplets with $T_j=145°C$.

fingers, N, based on Rayleigh–Taylor instability can be estimated by

$$N=\frac{D_s}{D_0}\sqrt{\frac{We}{12}}. \tag{26}$$

The maximum spread diameter has been replaced by the measured base diameter D_s, and the acceleration of liquid close to the contact line is assumed to be $\sim U^2/D_0$. Therefore, for $T_j=145°C$ and $L=1$ mm, $1<N<2$, less than the number of fingers observed in our tests. Therefore, fluid instabilities do not appear to be responsible for finger formation. Dhiman & Chandra[25] observed that splashing occurred at low substrate temperatures and disappeared at high substrate temperatures. Pasandideh-Fard et al.[26] found that splashing can be minimized by increasing thermal contact resistance. In our tests, the formation of the fingers could be triggered by the interactions of local solidification and spreading liquid near the contact line of spreading droplets. At the lowest substrate temperature ($T_s=60°C$), the viscosity of the ink would increase and prevent formation of fingers; at the highest substrate temperature ($T_s=80°C$), solidification around the rim would be delayed, minimizing the number of fingers.

CONCLUSIONS

Micrometer sized droplets of wax ink impacted on solid surface under various impact conditions produced different shapes and surface textures. Jetting temperature, substrate temperature and distance from printhead to substrate were varied to change impact conditions. Rough surfaces and irregular peripheries were formed when the substrate was closer from the printhead ($L=0.5$ mm), whereas smooth surfaces and peripheries were observed for droplets impacted at $L=1$ mm.

In our tests the oscillation and viscous damping times were comparable [Eq. (13)] and were much shorter than that for solidification of the entire droplet [Eqs. (8) and (17)]. This indicates the final shape can be predicted by evaluating the interaction of oscillation [Eq. (9)] and viscous damping [Eq. (11)]. Toward this end, one-dimensional heat conduction in a slab of finite thickness was considered for the spatio-temporal development of droplet temperature [Eq. (18)], and the temperature dependent viscosity and surface tension were taken into consideration [Eqs. (23) and (24)]. A transient Ohnesorge number [Eq. (22)] was introduced to compare the oscillation and damping time scales [Eqs. (9) and (11)] for the remaining liquid in the droplet. The number of tiers formed on the final shape can be predicted by the number of oscillations that are completed before the Ohnesorge number exceeds unity.

Two Marangoni numbers were defined to assess the thermal-capillary effect in the spreading [Eq. (15)] and post-spreading [Eq. (16)] phases of the droplet impact. It shows that the thermal-capillary effect is negligible during the spreading phase. For the test conditions with large values of post-spreading Marangoni number, the base diameter was measured to decrease with increasing substrate temperature. The thermal capillary effect may account for this trend.

For $T_j=145°C$ and $L=1$ mm, splashing occurred to form fingers around droplet peripheries. The number of fingers is more than the prediction based on Rayleigh–Taylor theory. The splashing was mainly caused by the interaction between the local solidification and spreading liquid around the droplet periphery.

ACKNOWLEDGMENTS

The authors are indebted to Farhad Farhadi for discussions related to this project and his valuable input. The authors are also indebted to Chris Wagner, Bradley Gerner and David Gervasi from Xerox Corporation for their assistance in setting up the jetting fixture. This work is supported by the Xerox Foundation and Natural Sciences and Engineering Research Council of Canada (NSERC).

NOMENTCLATURE

C_p = specific heat of droplet
D_0 = initial diameter of droplet
D_s = base diameter of droplet
$\hat{D}$ = length scale for Ohnesorge number $\hat{Oh}$
h = height of droplet
h_{sol} = thickness of solidified layer
k_d = thermal conductivity of droplet
k_s = thermal conductivity of substrate
L = distance of substrate from printhead
L_f = latent heat of fusion of droplet
N = number of fingers
R = radius
t_{damp} = viscous damping time
t_{imp} = impaction time
t_{osc} = oscillation time
t_{rec} = recoiling time

t_{sol} = solidification time
t_{spr} = spreading time
T = temperature
T_d = impact temperature of droplet
T_j = jetting temperature of printhead
T_m = effective melting temperature of droplet
T_s = substrate temperature
U = impact velocity of droplet
V_σ = capillary velocity
x = normal distance from substrate surface

Greek symbols

α_d = thermal diffusivity of droplet
λ = superheat parameter of droplet
μ = viscosity of droplet
μ_0 = viscosity of droplet at temperature T_d
$\hat{\mu}$ = mean viscosity of droplet
ρ = density of droplet
σ = surface tension of droplet
σ_0 = surface tension of droplet at temperature T_d
$\hat{\sigma}$ = mean surface tension of droplet

Dimensionless numbers

Ma_1 = Marangoni number in spreading phase
Ma_2 = Marangoni number in post-spreading phase
Oh = Ohnesorge number upon impact
$\hat{\mathrm{Oh}}$ = Ohnesorge number after impact
Pr = Prandtl number
Pe = Peclet number
Re = Reynolds number
Ste = Stefan number
We = Weber number

REFERENCES

[1] T. Snyder and S. Korol, "Modeling the offset solid-ink printing process," *Recent Progress in Ink Jet Technologies*, vol II (IS&T, Springfield, VA, 1999) pp. 175–181.
[2] H. P. Le, "Progress and trends in ink-jet printing technologies," J. Imaging Sci. Technol. **42**, 49–62 (1998).
[3] J. Madejski, "Solidification of droplets on a cold surface," Int. J. Heat Mass Transfer **19**, 1009–1013 (1976).
[4] S. D. Aziz and S. Chandra, "Impact, recoil and splashing of molten metal droplets," Int. J. Heat Mass Transfer **43**, 2841–2857 (2000).
[5] D. Attinger, Z. Zhao, and D. Poulikakos, "An experimental study of molten microdroplet surface deposition and solidification: Transient behavior and wetting angle dynamics," ASME J. Eng. Gas Turbines Power **122**, 544–556 (2000).
[6] F. C. Lee, R. N. Mills, and F. E. Talke, "The application of drop-on-demand ink jet technology to color printing," IBM J. Res. Dev. **28**, 307–313 (1984).
[7] S. Schiaffino and A. A. Sonin, "Molten droplet deposition and solidification at low Weber numbers," Phys. Fluids **9**(11), 3172–3187 (1997).
[8] F. Gao and A. A. Sonin, "Precise deposition of molten microdrops: The physics of digital micro-fabrication," Proc. R. Soc. London, Ser. A **44**, 533–554 (1994).
[9] J. W. S. Rayleigh, "On the capillary phenomena of jets," Proc. R. Soc. London **29**, 71–97 (1879).
[10] S. E. Bechtel, D. B. Bogy, and F. E. Talke, "Impact of a liquid drop against a flat surface," IBM J. Res. Dev. **25**(6), 963–971 (1981).
[11] R. Bhola and S. Chandra, "Parameters controlling solidification of molten wax droplets falling on a solid Surface," J. Mater. Sci. **34**, 4883–4894 (1999).
[12] M. Dietzel, S. Haferl, Y. Ventikos, and D. Poulikakos, "Marangoni and variable viscosity phenomena in picoliter size solder droplet deposition," ASME J. Eng. Gas Turbines Power **125**, 365–376 (2003).
[13] P. Ehrhard and S. H. Davis, "Non-isothermal spreading of liquid drops on horizontal plates," J. Fluid Mech. **229**, 365–388 (1991).
[14] P. Ehrhard, "Experiments on isothermal and non-isothermal spreading," J. Fluid Mech. **257**, 463–483 (1993).
[15] S. Harferl and D. Poulikakos, "Experimental investigation of the transient impact fluid dynamics and solidification of a molten microdroplet pile-up," Int. J. Heat Mass Transfer **46**, 535–550 (2003).
[16] J. M. Waldvogel and D. Poulikakos, "Solidification phenomena in picoliter size solder droplet deposition on a composite substrate," Int. J. Heat Mass Transfer **40**(2), 295–309 (1997).
[17] M. R. Predtechensky, Yu. D. Varlamov, S. N. Ulyankin, A. N. Cherepanov, and V. N. Popov, "Spreading and solidification of molten metal microdrops deposited on a substrate at moderate Weber numbers," J. Eng. Phys. Thermophys. **11**(1), 83–103 (2002).
[18] M. R. Predtechensky, Yu. D. Varlamov, S. N. Ulyankin, A. N. Cherepanov, and V. N. Popov, "Spreading and solidification of liquid metal droplets on a substrate: Experiment, analytical model, and numerical simulation," Int. J. Microcircuits Electron. Packag. **20**(4), 386–392 (2000).
[19] M. R. Predtechensky, A. N. Cherepanov, V. N. Popov, and Yu. D. Varlamov, "Crystallization dynamics of a liquid metal drop impinging onto a multilayered substrate," J. Appl. Mech. Tech. Phys. **43**(1), 93–102 (2002).
[20] M. Pasandideh-Fard, R. Bhola, S. Chandra, and J. Mostaghimi, "Deposition of tin droplets on a steel plate: Simulations and experiments," Int. J. Heat Mass Transfer **41**, 2929–2945 (1998).
[21] Z. Zhao, D. Poulikakos, and J. Fukai, "Heat transfer and Fluid dynamics during collision of a liquid droplet on a substrate-I. Modeling," Int. J. Heat Mass Transfer **39**(13), 2771–2789 (1996).
[22] J. R. A. Pearson, "On convection cells induced by surface tension," J. Fluid Mech. **4**, 489–500 (1958).
[23] C. H. Amon, K. S. Schmaltz, R. Merz, and F. B. Prinz, "Numerical and experimental investigation of interface bonding via substrate remelting of an impinging molten metal droplet," Int. J. Heat Mass Transfer **118**, 164–172 (1996).
[24] P. E. Bulavin and V. M. Kashcheev, "Solution of the non-homogeneous heat conduction equation for multilayered bodies," Int. Chem. Eng. **5**(1), 112–115 (1965).
[25] R. Dhiman and S. Chandra, "Freezing-induced splashing during impact of molten metal droplets with high Weber numbers," Int. J. Heat Mass Transfer **48**, 5625–5638 (2005).
[26] M. Pasandideh-Fard, V. Pershin, S. Chandra, and J. Mostaghimi, "Splat shapes in a thermal spray coating process: Simulations and experiments," J. Therm. Spray Technol. **11**, 206–217 (2002).